Published in Applied Physics Letters 84, 475-477, 2004
which should be used for any reference to this work

Terahertz range quantum well infrared photodetector

Marcel Graf,[a] Giacomo Scalari, Daniel Hofstetter, and Jérôme Faist
Institute of Physics, University of Neuchâtel, 1 A.-L. Breguet, 2000 Neuchâtel, Switzerland
Harvey Beere, Edmund Linfield, and David Ritchie
Cavendish Laboratory, University of Cambridge, Madingly Road, Cambridge, CB3 0HE United Kingdom
Giles Davies
School of Electronic and Electrical Engineering, University of Leeds, Leeds, LS2 9JT United Kingdom

We demonstrated a GaAs/AlGaAs-based far-infrared quantum well infrared photodetector at a wavelength of $\lambda=84$ μm. The relevant intersubband transition is slightly diagonal with a dipole matrix element of 3.0 nm. At 10 K, a responsivity of 8.6 mA/W and a detectivity of 5×10^7 cm $\sqrt{\text{Hz}}$/W have been achieved; and successful detection up to a device temperature of 50 K has been observed. Being designed for zero bias operation, this device profits from a relatively low dark current and a good noise behavior.

In recent years, there has been an increasing interest in the fabrication of so-called terahertz (THz) emitters and detectors. While electronic devices like Gunn diodes or Schottky diode frequency multipliers try to reach this range from the low frequency end, optical devices like gas or semiconductor lasers are quickly moving into the THz range from the high frequency side.[1–3] Since the THz region is traditionally defined as 0.1–3 THz, the currently available quantum cascade laser (QCL) sources with $\lambda=87$ μm can already be regarded as THz sources. At low temperatures, they emit several milliwatts of continuous wave output power. On the electronics side, Gunn diodes and frequency mixers have also achieved several milliwatts of radiated power at frequencies on the order of hundreds of gigahertz.[4] Once the entire THz frequency range is fully accessible by convenient radiation sources, it is obvious that the next important step towards applications is the development of suitable detectors. Like any other type of electromagnetic radiation, THz waves or pulses can be detected by coherent or incoherent means. Most coherent detection schemes utilize frequency conversion, whereas incoherent methods are based on the heat production of absorbed radiation. Typical examples of heat detectors include Si-bolometers or pyroelectric crystals like deuterated triglycerine-sulfate (DTGS); on the other hand, Schottky diode mixers,[5] nonlinear optical crystals like {110} ZnTe,[6] and gated photoconductive antennas are typical coherent detection schemes.[7] As a further incoherent solution, semiconductor-based quantum-type approaches like biased superlattices have attracted some attention.[8] Bolometers are in general highly sensitive, but like all heat-based detection schemes, they are intrinsically slow and built for very low temperature operation only.[9] DTGS detectors and pyroelectric crystals offer the advantage of faster detection at the prize of reduced sensitivity. Finally, extrinsic photoconductors such as doped Ge detectors are fast and sensitive, but they must be cooled to 4 K. Quite generally, coherent techniques profit from a good sensitivity, but they are experimentally more sophisticated than incoherent ones.[10] Although semiconductor quantum devices might not be highly sensitive, their potential for mass fabrication and integration by means of semiconductor device technology is very appealing. This has been proven by different types of quantum well infrared photodetectors (QWIPs) which work in a variety of different wavelength ranges.[11,12] By further exploiting the concept of using QCL-like structures as detectors,[13] we present here a THz detector based on a GaAs/AlGaAs based superlattice structure. The advantage of this approach is that electrons will be trapped in the subsequent active well as soon as they have made their contribution to the photocurrent; resulting in a good noise behavior. Although this happens at the cost of a small photoconductive gain, it is probably the most promising approach for a far-infrared QWIP.

Growth of the structures was based on molecular beam epitaxy on a semi-insulating GaAs substrate. On top of a 6000-Å-thick, n-doped (Si,2×10^{18} cm^{-3}) GaAs contact layer and a 200 Å undoped GaAs spacer layer, 60 periods of the following layers were grown (thicknesses in Å): **45**, 110, **40**, 135, **38**, 145, **36**, 180, **34**, 210, **15**, 100—where **bold** typeface denotes $Al_{0.15}Ga_{0.85}As$ barriers and roman GaAs wells; underlining marks the only n-doped (Si,6×10^{15} cm^{-3}) layer, resulting in an effective sheet carrier density of 8.7×10^9 cm^{-2}. After a last **45** Å barrier and another 200 Å spacer, 1000 Å n-doped (Si,2×10^{18} cm^{-3}) GaAs was deposited as top contact layer. The overall composition and the period of the superlattice were confirmed by x-ray diffraction. After growth, the samples were processed into square shaped mesas of different sizes (900, 450, 220 μm) using standard photolithography and wet etching with $H_2SO_4:H_2O_2:H_2O$ (ratio 1:8:1). The first deposited metallization in the area outside the mesas, 100/350 nm thermally evaporated GeAu/Au, was annealed at 400 °C for 60 s and served as bottom ohmic contact. On top of the mesas, we evaporated a 100-nm-thick metallic grating (GeAu) with a period of 15 μm. This was then partly covered by another metallization layer (Cr/Au, 10/200 nm) to enable subsequent wire bonding for the top contact. These top metal layers were annealed at 320 °C for 60 s. The sample was soldered on a copper submount and its top contacts were bonded to Au-coated ceramic contact pads. The bottom contact was con-

[a]Electronic mail: marcel.graf@unine.ch

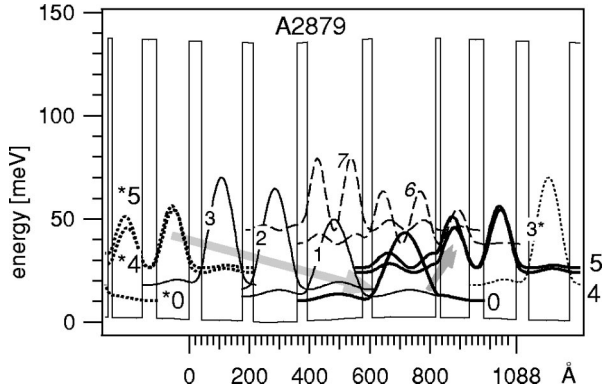

FIG. 1. Self-consistently calculated conduction band structure of A2879 at 10 K. One full period, surrounded by adjacent parts of the previous/next period, is shown. The observed transitions take place between the ground state 0 and the states 4 and 5 and have computed energies of 13.7 and 16.0 meV. The states 3, 2, and 1 provide the relaxation channel for the electrons to the ground state of the next period.

nected directly to the copper submount. All experiments were done with the sample held on the cold finger of a liquid He-flow cryostat. Spectral photocurrent measurements were done with a Nicolet Fourier-transforming infrared spectrometer (FTIR) using the internal glowbar as the light source. The sample was placed at the focus of an $f/2.0$ beam condenser in the sample compartment and illuminated on its top face where the diffraction by the grating provided optical coupling to the active layers. Similar results were obtained by illuminating from the side through a 45° polished facet. The signal was amplified by an EG&G voltage preamplifier and fed back to the FTIRs internal circuitry. In the case of applied bias voltages, the sample was connected in series with a resistance acting as current–voltage converter—otherwise, the device was directly connected to the preamplifier, thus effectively using the internal resistance of the device as transimpedance. Responsivity measurements were carried out by illuminating the sample with an 87 μm QCL whose intensity versus current (L–I) curve had been previously measured with a thermopile powermeter.[14] Finally, dark current measurements were done with a Keithley 2400 SourceMeter at different temperatures between 6 and 150 K.

In Fig. 1, we present a self-consistently computed conduction band diagram of our structure. The calculated ener-

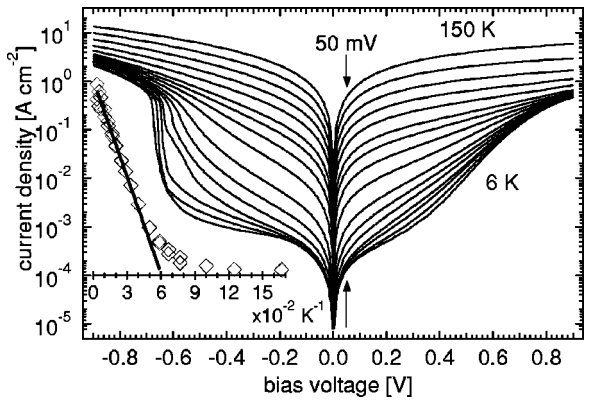

FIG. 2. Measurements of I–V characteristics at temperatures of 6, 8, 10, 13, 15, 17, 20, 25, 30, 35, 40, 50, 60, 75, 100, and 150 K. The inset shows an Arrhenius plot ($\diamond$) of current densities at 50 mV bias. The solid line is a fit resulting in an activation energy of 13.2 meV which is in good agreement with the (0→4) transition energy of 13.7 meV.

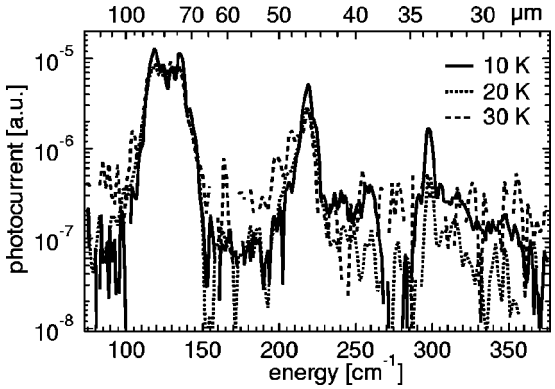

FIG. 3. Photocurrent spectra of the device, illuminated with blackbody radiation from the internal glowbar of the FTIR. The different peaks can be identified with calculated transition energies.

gies for the diagonal transitions from the ground state 0 up to states 4 or 5 are 13.7 and 16.0 meV. We also observed the transitions from 0 to 6 and from 0 to 7, their calculated energies are 27.5 and 34.2 meV. Once excited into state 4 or 5, the electrons have a certain tunneling probability to state 3, from where they ''slide'' down to the ground state of the next period (→3→2→1→0), effectively contributing to photocurrent. The device is therefore designed to work under zero bias conditions, which avoids additional noise due to dark current.

Figure 2 shows dark current measurements carried out at different temperatures. The region with a substantially reduced differential resistance around −0.65 V bias corresponds to the situation where the upper state of the transition (0→4) is resonantly aligned with the ground state of the next period (''lasing''-type of bandstructure). From the Arrhenius plot displaying logarithmic dark current at a constant voltage (50 mV) versus inverse temperature (inset of Fig. 2), an activation energy of 13.2 meV could be extracted; this agrees well with the smallest calculated transition energy (0→4, 13.7 meV). For temperatures below 20 K, a temperature independent component of the dark current gets dominant, which we attribute to direct tunneling processes across the structure.

Spectral photocurrent measurements, as shown in Fig. 3, prove the usability of the sample as detector. The large peaks at 119 cm^{-1} (84 μm) and 135 cm^{-1} (74 μm) are at the expected energies (110 and 129 cm^{-1} from simulation). In this configuration, we were able to detect the glowbar up to a detector temperature of 30 K. Additional peaks at 219 and 297 cm^{-1} are likewise identified as transitions into states 6 and 7. With rising device temperature from 10 to 30 K, the constant photocurrent signal gets more and more buried in the rising noise floor until it is completely concealed above 30 K.

Determination of the detector responsivity was done using a bound-to-continuum QCL at 87 μm. The light from the laser was picked up directly on the outside of the laser cryostat window and guided to the detector cryostat through a gold-coated lightpipe. For a total mean output power of 350 μW at this place (measured with a thermopile powermeter), we first performed a lateral scan by moving the detector cryostat. Assuming circular symmetry and integrating the radial intensity profile over the entire aperture of the lightpipe al-

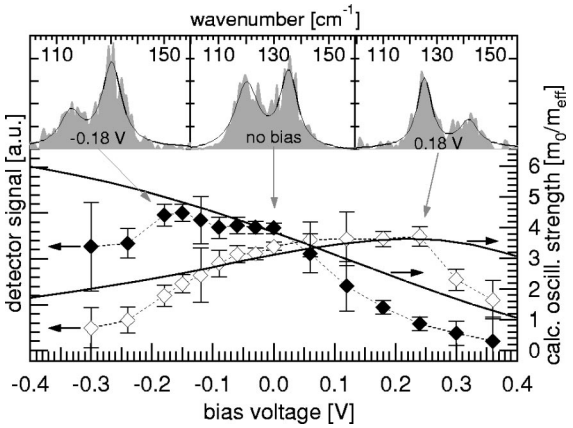

FIG. 4. Bias voltage dependent ratio between the first two transitions (0→4 and 0→5). The solid curves were obtained from bandstructure simulations, the dashed curves are the result of spectral photocurrent measurements at different bias voltages. The insets show three of these measurements at −0.18, 0, and +0.18 V bias together with the fitted double peak Lorentzians.

lowed us to calculate the total power (in the center of the pipe) illuminating the sample surface. Together with the photocurrent from the device, which was measured with the current input of an EG&G 7260 lock-in amplifier triggered by the laser pulser, a responsivity $R=8.6$ mA/W at 10 K detector temperature was calculated. To estimate the noise equivalent power (NEP), we performed an $L-I$ characterization of the same laser, using our device as detector. Calibration was done again with the powermeter, using exactly the same setup as before. At a NEP of 7 nW, the growing signal during switch-on of the laser rose above noise level, therefore a detectivity D^* of 5×10^7 cm $\sqrt{\text{Hz}}$/W was determined. Compared to the performance (at 84 μm) of a heterojunction terahertz detector based on internal photoemission,[15] responsivity and detectivity of our device are roughly two orders of magnitude lower. On the other hand, a 60 period photodetector with 100% internal quantum efficiency would theoretically result in a responsivity of 1.15 A/W (one electron has to absorb 60 photons to pass the whole structure).

Based on dipole matrix elements from the numerical simulation, we expect the device to have an intersubband absorption of about $\eta=3\%$ for both relevant transitions (0→4,5). From the fact that states 4 and 5 are (too) strongly coupled, which is confirmed by the observered anticrossing behavior under applied bias voltage (Fig. 4), and due to the coherent tunneling of the electrons between these two states, we estimate an escape probability of $p_e\approx0.5$. Together with a capturing probability $p_c=1$ due to the particular design, we would expect a maximum responsivity $R_i=(e/h\nu)\,\eta g_{\text{photo}}=(e/h\nu)\,\eta p_e/(Np_c)=18$ mA/W.[16]

Despite we confirmed the intended doping level using capacitance–voltage measurements from our structure, absorption was too weak to yield a reliable result (<2%), even in a multipass (four passes) waveguide geometry. One possibility is that a substantial fraction of the n-type carriers is trapped by impurities below the ground state and therefore not available for absorption, as the overall dopant concentration of 8×10^{14} cm^{-3} is in the same order of magnitude as the background doping. Furthermore, the coupling through the top-illuminated diffraction grating might be quite inefficient. Yet, using a QCL as the light source enabled us to detect radiation up to a detector temperature of 50 K; mainly thanks to the higher brightness of the laser compared to the glowbar.

As mentioned before, this detector was designed for operation under zero bias conditions. Accordingly, applying bias voltages did not improve its performance compared to the unbiased situation. Nevertheless, it allowed us to verify whether the device shows a Stark shift as expected from theoretical predictions. Figure 4 shows calculated oscillator strengths for the main transitions 0→4 and 0→5 as function of applied voltage (solid) and in comparison with measured values (dashed). The measured points were obtained by fitting the double peaks in the photocurrent spectra by two Lorentzians; three examples at different bias voltages are shown as insets. When the field changes from negative to positive values, the oscillator strength of the 0→4 transition increases at the cost of the decreasing 0→5 transition. As presented in Fig. 4, this Stark effect was clearly visible in both experiment and simulation.

In summary, a GaAs/AlGaAs-based QWIP detecting at 3.5 THz was demonstrated. It is based on a QCL-like band structure and we successfully operated the device in a temperature range between 10 and 50 K. At the wavelength $\lambda=84$ μm and a device temperature of 10 K, a responsivity of 8.6 mA/W and a detectivity of 5×10^7 cm $\sqrt{\text{Hz}}$/W have been achieved. Based on the results obtained with this detector, we believe that an improved fabrication process and a careful redesign, especially increasing the doping density and engineering of the involved oscillator strength, will result in a performance improvement in terms of both operating temperature and detectivity.

The authors gratefully acknowledge financial support from the Professorship Program of the Swiss National Science Foundation, the NICOP program of the US Office of Naval Research, and the European Research Project WANTED.

[1] R. Köhler, A. Tredicucci, F. Beltram, H. Beere, G. Davies, E. Linfield, and D. Ritchie, Nature (London) **417**, 156 (2002).
[2] L. Ajili, G. Scalari, D. Hofstetter, M. Beck, J. Faist, H. Beere, G. Davis, E. Linfield, and D. Ritchie, Electron. Lett. **38**, 1675 (2002).
[3] R. Köhler, A. Tredicucci, F. Beltram, H. E. Beere, E. H. Linfield, D. A. Ritchie, and A. G. Davies, Electron. Lett. **39**, 1254 (2003).
[4] W. H. Haindl, S. Smith, and R. Bosch, Appl. Phys. Lett. **37**, 556 (1980).
[5] D. T. Hodges and M. McColl, Appl. Phys. Lett. **30**, 5 (1977).
[6] Z. Jiang and X.-C. Zhang, Appl. Phys. Lett. **72**, 1945 (1998).
[7] Y. Cai, I. Brener, J. Lopata, J. Wynn, L. Pfeiffer, J. B. Stark, Q. Wu, X. C. Zhang, and J. F. Federici, Appl. Phys. Lett. **73**, 444 (1998).
[8] F. Klappenberger, A. A. Ignatov, S. Winnerl, E. Schomburg, W. Wegscheider, K. F. Renk, and M. Bichler, Appl. Phys. Lett. **78**, 1673 (2001).
[9] J. P. Rice, E. N. Grossman, and D. A. Rudman, Appl. Phys. Lett. **65**, 773 (1994).
[10] R. E. Drullinger, K. M. Evenson, D. A. Jennings, F. R. Petersen, J. C. Bergquist, L. Burkins, and H.-U. Daniel, Appl. Phys. Lett. **42**, 137 (1983).
[11] H. C. Liu, R. Dudek, A. Shen, E. Dupont, C. Y. Song, Z. R. Wasilewski, and M. Buchanan, Appl. Phys. Lett. **79**, 4237 (2001).
[12] S. D. Gunapala, S. V. Bandara, J. K. Liu, W. Hong, M. Sundaram, P. D. Maker, R. E. Muller, C. A. Shott, and R. Carralejo, IEEE Trans. Electron Devices **45**, 1890 (1998).
[13] D. Hofstetter, M. Beck, and J. Faist, Appl. Phys. Lett. **81**, 2683 (2002).
[14] G. Scalari, L. Ajili, J. Faist, H. Beere, E. Linfield, D. Ritchie, and G. Davies, Appl. Phys. Lett. **82**, 3165 (2003).
[15] S. G. Matsik, M. B. M. Rinzna, A. G. U. Perera, H. C. Liu, Z. R. Wasilewski, and M. Buchanan, Appl. Phys. Lett. **82**, 139 (2003).
[16] H. C. Liu, in *Intersubband Transitions in Quantum Wells: Physics and Device Applications I*, Semiconductors and Semimetals Vol. 62, edited by H. C. Liu and F. Capasso (Academic, San Diego, 2000), p. 154.